OXFORD JOURNAL
OF STUDENT
SCHOLARSHIP

When Does a Wheatstone Bridge Outperform a Voltage Divider? A Sensitivity-Based Modeling and Simulation Study

Tri Tran
tritran1737@gmail.com

ABSTRACT

Resistive sensors are widely used in instrumentation, but converting small resistance changes (ΔR) into useful voltage signals can be complicated by excitation-voltage variation and other nonidealities. This study compares a simple voltage divider and a quarter-active Wheatstone bridge through normalized analytical models and finite-difference simulations. A dimensionless efficiency metric, $E(\theta, \varphi)$, is defined as the magnitude of sensitivity to normalized resistance variation (θ) divided by sensitivity to normalized excitation-voltage variation (φ). Across a 10-by-15 grid spanning $\theta, \varphi \in [0.1, 5.0]$, the pointwise bridge-to-divider efficiency ratio ranges from 2.4 to 22 and has a mean of 4.95. The ratio is independent of φ in the ideal model and increases without bound as θ approaches zero because the balanced bridge has zero output and zero first-order excitation sensitivity at that exact operating point. These results describe the selected absolute-output metric, not universal signal-to-noise superiority: resistor mismatch, drift, amplifier behavior, quantization, ratiometric conversion, and divider baseline subtraction are outside the model. Within those limits, the framework provides a reproducible way to compare how the two topologies trade sensitivity to resistance change against sensitivity to excitation variation. The bridge's larger ratio partly reflects its zero output at balance. Here, "efficiency" means a sensitivity ratio, not electrical power efficiency.

Keywords: *Wheatstone bridge, voltage divider, resistive sensors, sensitivity analysis, parameter sweep, sensor interface circuits, finite-difference methods*

INTRODUCTION

Resistive sensors are among the most widely used sensing technologies because of their low cost, simple construction, and ability to measure many physical quantities, including temperature, force, pressure, displacement, and light intensity (Chiang et al., 2018; Jan et al., 2024; Liu et al., 2018; Zhu et al., 2022). In a measurement system, the resistance change ΔR produced by a sensor must be converted into an electrical signal that can be processed by analog or digital circuitry. Resistance-to-voltage converters therefore form a foundational part of many sensor interfaces (Wilson, 2022; Yermoshin et al., 2021).

Many resistive sensors generate small fractional resistance changes. The resulting signals must be distinguished from supply variation, component tolerance, temperature drift, readout offset, quantization, and electrical noise (De Marcellis & Ferri, 2011; Wilson, 2022). Consequently, the topology and readout method can materially affect the accuracy and reliability of a sensing system. In the comparison below, the bridge's zero differential output at balance suppresses excitation sensitivity, while the divider retains a nonzero absolute baseline. This difference in output definition contributes directly to the bridge's larger sensitivity ratio.

The application context also matters. Flexible and wearable sensors emphasize mechanical compliance and low-cost integration, tactile sensors emphasize repeatable detection of contact or slip, and environmental monitors must convert a material response into an electrical quantity that can be digitized (Chiang et al., 2018; Jan et al., 2024; Liu et al., 2018). Although these devices differ physically, their readout circuits face the same basic problem: the desired resistance-dependent voltage must remain distinguishable from changes introduced by the excitation source and the rest of the signal chain. A topology comparison is therefore useful only when its output definition, disturbance model, and operating point are stated explicitly.

Two classical passive topologies are the voltage divider and the Wheatstone bridge (Kester, 1999; Wilson, 2022). The voltage divider has a low component count and is useful when simplicity is important or resistance changes are large. Its absolute output scales with excitation voltage. In a non-ratiometric readout, excitation variation therefore appears directly in the measured voltage; in a ratiometric analog-to-digital conversion that uses the same source as its reference, much of this dependence can instead cancel.

The Wheatstone bridge uses the difference between two divider arms. At balance, its ideal differential output is zero. A small resistance change in one arm creates a differential output, while excitation variation alone produces no first-order differential output at the exact balanced point. This property supports high-precision applications such as strain-gauge load cells, pressure transducers, and industrial instrumentation (Azadmehr et al., 2017; Kester, 1999; Texas Instruments, n.d.). Away from balance, however, the bridge output also scales with excitation, so the degree of rejection depends on operating point and readout architecture.

Standard treatments describe the two topologies and their practical readout contexts (Kester, 1999; Wilson, 2022). A normalized comparison can make their different operating-point behavior more explicit. This study derives input-output models for both topologies, defines a dimensionless efficiency metric that compares sensitivity to the desired resistance change with sensitivity to excitation variation, and maps that metric over a common parameter grid. The research question is therefore narrow: under the specified ideal absolute-output model, where does the Wheatstone bridge produce a larger desired-to-disturbance sensitivity ratio than the voltage divider?

This question differs from asking which circuit is universally more accurate. Accuracy requires an error budget that includes the source, sensor, resistors, amplifier, converter, calibration procedure, and environment. This analysis does not include those factors and instead focuses on one mathematical difference: the divider has a nonzero absolute baseline at nominal resistance, whereas the balanced bridge subtracts two equal arm voltages and has a zero differential baseline. The resulting metric is best understood as an analytical result that later models can extend.

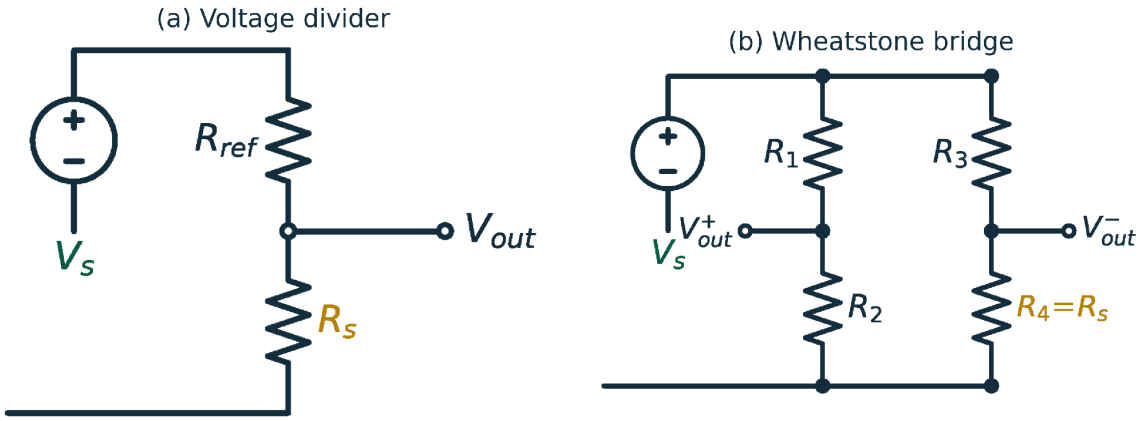


Figure 1. Resistance-to-voltage topologies compared in this study: (a) a voltage divider with a single-ended output and (b) a quarter-active Wheatstone bridge with a differential output. The terminal labels in panel (b) use left-minus-right polarity; Equation 2 and the numerical model use right-minus-left polarity. Reversing polarity does not affect the absolute sensitivity metric.

THEORETICAL BACKGROUND AND SENSITIVITY FRAMEWORK

Resistance-to-Voltage Conversion

The interface must translate a resistance change into a measurable voltage while preserving the information carried by the sensor. This study isolates one disturbance, excitation-voltage variation, and holds all resistors other than the active sensor at their nominal values. Other error sources are treated as limitations rather than simulated variables.

For the voltage divider, a reference resistor Rref is placed in series with sensor resistance Rs and driven by excitation V_s. Taking the output across the sensor gives

$$V_{out,div} = V_s \frac{R_s}{R_{ref} + R_s} \tag{1}$$

so both resistance and excitation voltage affect the absolute output.

For the bridge, V_s is applied across two resistor arms and the output is their voltage difference. Defining the modeled output as the right midpoint minus the left midpoint (opposite to the terminal polarity labels in Figure 1) gives

$$V_{out,bridge} = V_s \left(\frac{R_4}{R_3 + R_4} - \frac{R_2}{R_1 + R_2} \right) \tag{2}$$

When R1 = R2 = R3 = R4, the bridge is balanced and the differential output is zero.

Scope of the Comparison

Equations 1 and 2 compare the raw absolute outputs shown in Figure 1. The divider output is not shifted by its nominal value, and the bridge is represented by one active resistance in a four-resistor network. This choice corresponds to a quarter-active bridge, not a half- or full-active strain-gauge bridge. It also does not include an instrumentation amplifier or analog-to-digital converter. These definitions are necessary because adding baseline subtraction, gain, or a shared voltage reference can change the apparent sensitivity to excitation.

The bridge should therefore not be interpreted as creating energy or an infinite signal. It creates a differential, zero-centered representation of imbalance. That representation can be convenient for high-gain differential amplification, but the bridge still consumes excitation power and its nonzero output away from balance remains proportional to V_s. The divider is likewise not inherently unsuitable for precision work: with stable excitation, calibration, and ratiometric conversion, it can provide accurate measurements. The models isolate only how the two raw outputs respond locally to θ and φ.

Normalized Variables and Efficiency Metric

Let R_0 denote nominal resistance and Vs0 nominal excitation. The dimensionless signal and disturbance variables are

$$\theta = \frac{\Delta R}{R_0}, \qquad \phi = \frac{\Delta V_s}{V_{s0}} \tag{3}$$

with $R_s = R_0 (1 + \theta)$ and $V_s = V_{s0} (1 + \varphi)$. Because the nominal excitation cancels from the final comparison, Vs0 is set to one. The normalized output of each topology is denoted h(θ, φ). Equivalently, h is the circuit output divided by the nominal excitation V_{s0}.

The efficiency metric is

$$E(\theta, \phi) = \frac{\left| \frac{\partial h}{\partial \theta} \right|}{\left| \frac{\partial h}{\partial \phi} \right|} \tag{4}$$

and quantifies desired-signal sensitivity relative to excitation sensitivity at a specified operating point. Larger E means that a local change in normalized resistance produces a larger output change relative to the output change caused by a local normalized excitation variation. The quantity is not a complete noise, accuracy, or signal-to-noise metric because it excludes all disturbances other than φ. Here, "efficiency" means only this dimensionless desired-to-excitation sensitivity ratio; it does not mean electrical power efficiency or conversion efficiency.

For a non-ratiometric sensor readout, this ratio can support an excitation-error budget. Linearizing at a chosen operating point gives a desired output change $|\partial h/\partial \theta|\,|\delta\theta|$ and an excitation-induced output change $|\partial h/\partial \varphi|\,|\delta\varphi|$. Their ratio is $E|\delta\theta|/|\delta\varphi|$. Equivalently, the excitation disturbance corresponds locally to an apparent normalized resistance error $|\delta\theta_{eq}| = |\delta\varphi|/E$ when interpreted through the resistance sensitivity. Thus, a larger E reduces the equivalent input error for a specified small excitation disturbance under the model. Actual signal and disturbance magnitudes must still be supplied; E alone is not a signal-to-noise ratio.

For $R_{ref} = R_0$, the divider model becomes

$$h_{div}(\theta, \phi) = (1 + \phi)\frac{1 + \theta}{2 + \theta} \tag{5}$$

For a quarter-active bridge with $R_1 = R_2 = R_3 = R_0$ and $R_4 = R_0 (1 + \theta)$,

$$h_{bridge}(\theta, \phi) = (1 + \phi)\left(\frac{1 + \theta}{2 + \theta} - \frac{1}{2}\right) = \frac{(1 + \phi)\theta}{2(2 + \theta)} \tag{6}$$

Differentiating Equations 5 and 6 and applying Equation 4 gives

$$E_{div} = \left| \frac{1 + \phi}{(1 + \theta)(2 + \theta)} \right| \tag{7}$$

and

$$E_{bridge} = \left| \frac{2(1 + \phi)}{\theta(2 + \theta)} \right| \tag{8}$$

The pointwise efficiency ratio is therefore

$$R_E = \frac{E_{bridge}}{E_{div}} = \frac{2|1 + \theta|}{|\theta|} \tag{9}$$

Equation 9 is independent of φ. As $\theta \to 0$, the ratio becomes unbounded; at exactly $\theta = 0$, both the bridge output and its derivative with respect to excitation are zero, so Equation 4 has a zero

denominator and E_{bridge} is undefined. This mathematical singularity represents the ideal, perfectly balanced limit rather than an infinite physical signal. Real mismatch, offset, noise, and finite resolution prevent an actual circuit from achieving the ideal divergence, and the simulation avoids the undefined point by starting at $\theta = 0.1$.

METHODS

Computational Tools

Numerical differentiation and figure generation were implemented in Python using NumPy and Matplotlib (Harris et al., 2020; Hunter, 2007). Separate output functions represented the divider and bridge. Each sensitivity was evaluated with a forward finite difference, after which the absolute derivative magnitudes were divided according to Equation 4. The complete code used for Figures 3 and 4 is reproduced in Appendix A.

Parameter Space

The simulation used 10 evenly spaced values of θ and 15 evenly spaced values of φ, each over [0.1, 5.0], for 150 operating points. These broad dimensionless ranges were selected to show the overall behavior and limits of the metric. They should be interpreted as a selected normalized parameter range, not as a claim that a 500% excitation change represents a typical regulated supply tolerance. Likewise, the upper portion of the θ range represents large resistance excursions rather than small-signal bridge operation. In particular, $\theta = 5$ and $\varphi = 5$ mean six times the nominal resistance and excitation, respectively (a 500% increase). The upper limits illustrate the mathematical trend and are not recommended sensor operating conditions.

Finite-Difference Approximation

Forward finite differences with step $h = 10^{-10}$ approximated the two partial derivatives:

$$\frac{\partial h}{\partial \theta} \approx \frac{h(\theta + h, \phi) - h(\theta, \phi)}{h}, \qquad \frac{\partial h}{\partial \phi} \approx \frac{h(\theta, \phi + h) - h(\theta, \phi)}{h} \tag{10}$$

Although the derivatives are available analytically for the ideal equations, numerical differentiation also allows the same method to be used with future nonlinear or temperature-dependent models. The analytical expressions in Equations 7-9 serve as the reference for interpreting the numerical surfaces. The step $h = 10^{-10}$ is very small relative to the normalized variables and limits forward-difference truncation error in exact arithmetic, but it was not established as an optimal step. In floating-point arithmetic, subtracting nearly equal outputs can amplify rounding error. To check this tradeoff, the calculation was repeated with $h = 10^{-4}$, 10^{-6}, 10^{-8}, and 10^{-10} over the same 150-point grid. Table 2 reports the maximum relative error against Equations 7–9, defined as $100 \times \max|Q_{num}/Q_{exact} - 1|$ for each reported quantity Q. The added check uses NumPy 2.3.5 and double precision. Figures 3–4 and Table 1 keep the original $h = 10^{-10}$. This checks the calculation, not physical circuit performance.

Response Surface and Summary Statistics

The same grid and plotting procedure were applied to both topologies. Efficiency values were summarized by their maximum, minimum, mean, median, and population standard deviation over all 150 grid points. The same statistics were calculated for the pointwise ratio RE ; the ratio column in Table 1 therefore describes the distribution of Ebridge / Ediv across grid points, not the quotient of the other columns' summary statistics.

For reproducibility, the algorithm followed the equations in a fixed sequence. It first generated the θ and φ arrays, evaluated both normalized output functions at each grid point, estimated the two partial derivatives, and formed E only after taking absolute derivative magnitudes. The resulting two efficiency arrays were then used for the surfaces and descriptive statistics. A separate script divided the bridge array by the divider array point by point and compared the result with Equation 9. No random values, fitted parameters, or external data files were used, so repeated executions with the listed software dependencies should produce the same arrays apart from normal floating-point differences.

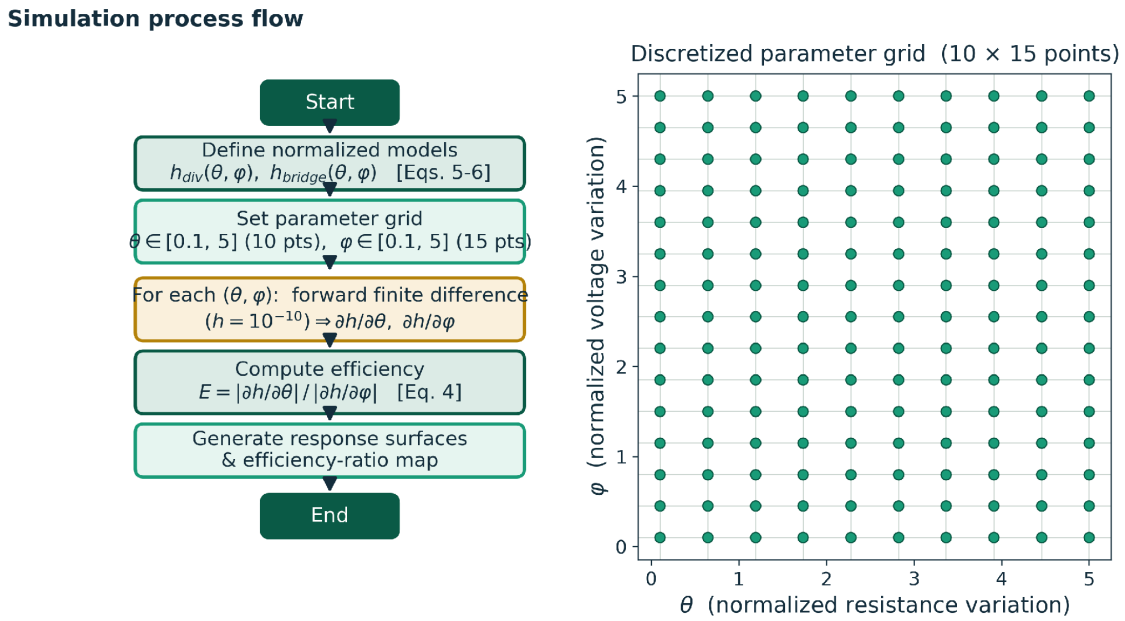


Figure 2. Computational workflow and the discretized 10-by-15 parameter grid used for both circuit models.

RESULTS

Efficiency Response Surfaces

Figure 3 shows E(θ, φ) for the voltage divider and Wheatstone bridge. In both topologies, efficiency increases with φ under the defined metric because the desired-signal derivative contains the factor 1 + φ. Efficiency decreases as θ increases. The bridge surface is substantially higher near the balanced limit, where its sensitivity to excitation variation is proportional to the small imbalance θ.

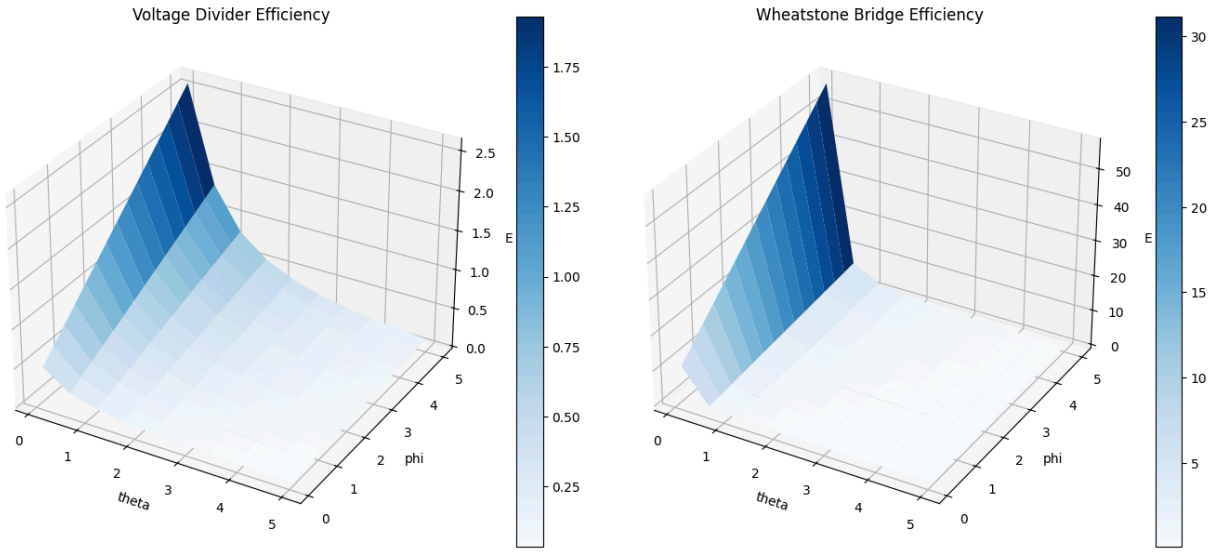


Figure 3. Efficiency response surfaces over the parameter grid: (a) voltage divider and (b) Wheatstone bridge. The vertical scales differ and should be read from their respective axes and color bars. All plotted variables are dimensionless.

Table 1 reports statistics over the 150 simulated points. The pointwise bridge-to-divider ratio ranges from 2.4 to 22, with a mean of 4.95 and a median of 2.79. Thus, the bridge is not more than one order of magnitude higher at every point; an order-of-magnitude difference occurs only at the smallest sampled θ value.

Table 1. Summary statistics for the dimensionless efficiency metrics and pointwise bridge-to-divider ratio over 150 grid points.

Statistic	**Voltage divider E_{div}**	**Wheatstone bridge E_{bridge}**	**Pointwise Ratio R_E**
Maximum	2.60	57.14	22.00
Minimum	0.026	0.063	2.40
Mean	0.411	4.33	4.95
Median	0.209	0.583	2.79
Population standard deviation	0.502	10.91	5.74

Efficiency-Ratio Map

Figure 4 directly visualizes RE. The vertical contours in panel (a) confirm that the ratio is independent of φ, as Equation 9 predicts. In panel (b), numerical values at three φ levels lie on the same closed-form curve. The ratio is 22 at θ = 0.1 and decreases monotonically to 2.4 at θ = 5.0.

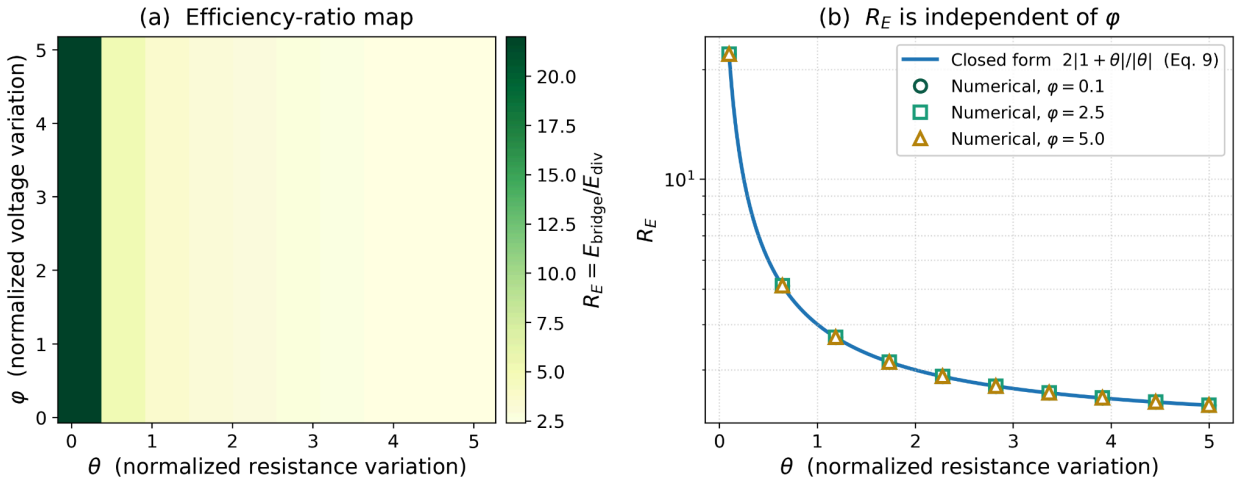


Figure 4. Pointwise efficiency ratio RE = Ebridge/Ediv : (a) map over the parameter plane and (b) numerical values at three excitation levels overlaid on Equation 9.

Agreement between the numerical and analytical results provides an internal implementation check. Forward differences approximate two smooth rational functions, while Equation 9 follows independently from symbolic differentiation of the same ideal output equations. The three numerical traces in Figure 4(b), evaluated at φ = 0.1, 2.5, and 5.0, coincide with the closed-form curve across the sampled θ values within plotting resolution. This agreement confirms that the grid orientation, derivative definitions, and ratio calculation were implemented consistently; it also explains why the φ dependence in the individual efficiency surfaces cancels in the topology ratio. Because h = 10^{-10} is small relative to the modeled quantities, the finite-difference calculation could in principle be affected by floating-point cancellation, making the closed-form overlay a useful numerical sanity check. This check is not physical validation: both calculations inherit the same ideal assumptions and cannot reveal omitted tolerance, noise, or loading effects. Its purpose here is to check that the reported trend does not result from a plotting or indexing error.

Table 2 shows that the largest error in R_E is below 0.0069% for every tested step. Errors in E_{div} and E_{bridge} are each below 0.0055%. The same overall trend therefore holds across all four steps. Among the tested choices, h = 10^{-6} gives the lowest maximum error for both individual metrics. Smaller steps are therefore not always more accurate. Some errors cancel when the two metrics are divided, so an accurate ratio alone does not guarantee equally accurate individual metrics. These checks do not test noise, component tolerances, or the readout electronics.

Table 2. Maximum relative error (%) against the analytical formulas over the 150-point grid. All four steps use forward differences and double precision.

Step h	**E_{div} error (%)**	**E_{bridge} error (%)**	**RE error (%)**
1e-4	0.00476	0.00476	5.73e-9
1e-6	4.77e-5	4.77e-5	6.46e-7
1e-8	5.82e-5	5.30e-5	7.53e-5
1e-10	0.00546	0.00338	0.00687

DISCUSSION

Interpretation of the Metric

Under the ideal equations and the absolute-output efficiency metric, the quarter-active bridge has a larger desired-to-excitation sensitivity ratio than the divider at every sampled point. The result follows analytically from Equation 9 rather than from a general property that holds for every readout implementation. At balance, the bridge's differential baseline is zero, so a supply change alone produces no ideal differential output. The divider, by contrast, has an absolute baseline of approximately one-half the excitation voltage, which gives it nonzero excitation sensitivity even when θ is small.

This distinction is important for practical interpretation. Subtracting a fixed nominal voltage from the divider output leaves its response to excitation changes unchanged. Subtracting half of the actual excitation voltage, $V_s/2$, gives the same ideal output as the quarter-active bridge. A ratiometric readout divides the measured output by a reference voltage that follows the excitation. This cancels the excitation dependence in the ideal model. The comparison therefore depends on the readout method. The present metric also does not include noise spectral density, amplifier common-mode rejection, output impedance, power, calibration, bandwidth, or component count. The findings therefore support a conditional claim: the bridge is favored by the defined local absolute-output sensitivity ratio in the ideal quarter-active model.

Because the metric depends on the chosen output definition, its conclusions are limited to the model used here. Sensitivity ratios are useful when the numerator and denominator correspond to the disturbances that matter in a specific design. Here, ϕ represents fractional excitation change and no other nuisance variable. If thermal drift were added, for example, the denominator would need an additional sensitivity term or a multivariable error model. If white and flicker noise were added, spectral densities and bandwidth would be required rather than partial derivatives alone. The response surfaces therefore answer a defined local-sensitivity question and should not be relabeled as measured accuracy or signal-to-noise ratio.

Illustrative strain gauge example

For an illustrative strain-gauge example, assume a nominal resistance $R_0 = 350\ \Omega$, gauge factor $G = 2$, strain $\varepsilon = 500$ microstrain, and nominal excitation $V_{s0} = 5$ V. These values are chosen for illustration and are not experimental data. The gauge-factor relation $\theta = G\varepsilon$ gives $\theta = 0.001$ and $\Delta R = 0.35\ \Omega$. At nominal excitation ($\varphi = 0$), Equations 5–6 give a divider output of about 2.501249 V and a bridge output of 1.249 mV. Compared with their outputs at $\theta = 0$, both circuits produce the same 1.249 mV change due to strain.

Now increase excitation by 0.1% while keeping strain fixed ($\delta\varphi = 0.001$). The divider output changes by about 2.501 mV, while the bridge output changes by about 1.249 μV. The ratio of these excitation-induced changes is 2002, equal to Equation 9 at $\theta = 0.001$. Both circuits have the same derivative $\partial h/\partial\theta$, so this larger ratio comes from the bridge's smaller absolute output rather than a larger response to strain. The

example uses a resistance change below the sweep's lower limit of $\theta = 0.1$. It shows how a small bridge baseline can reduce output error from supply changes. Noise, resistor mismatch, and amplifier behavior must still be considered in a practical design.

Relation to Prior Work

Bridge and divider front ends are well established in sensor-interface literature. Wilson (2022) surveys resistance-based interface circuits, Azadmehr et al. (2017) describe a virtual bridge front end, and De Marcellis and Ferri (2011) discuss broader voltage- and current-mode sensor interfaces. Texas Instruments (n.d.) and Kester (1999) document practical bridge measurement and signal-conditioning considerations. Van Rethy et al. (2013) present a supply-noise-resilient force-balanced bridge interface. These sources support the qualitative importance of differential bridge sensing but do not use the exact efficiency metric defined here. Accordingly, this study does not claim quantitative agreement with those works; its contribution is the explicit normalized ratio in Equation 9 and its visualization over a common parameter domain.

Limitations and Future Work

This is an idealized, simulation-only comparison. It assumes exact nominal resistors, a single active bridge arm, noiseless and infinite-impedance voltage measurement, and no lead resistance. It excludes resistor mismatch, temperature coefficients, self-heating, source impedance, amplifier input offset and bias, common-mode limits, quantization, electromagnetic interference, and calibration error. These effects can create a nonzero bridge output at nominal balance and eliminate the mathematical divergence described above. No laboratory experiment was performed, so the results should not be presented as measured circuit performance.

The parameter grid is also intentionally broad and coarse. Values up to $\theta = 5$ are outside the small-signal regime typical of many strain-gauge bridges, and $\varphi = 5$ is a normalized stress-test value rather than a representative supply tolerance. Because Equation 9 is independent of φ and monotonic in θ, the coarse grid is adequate for visualizing the ideal surface, but it does not establish engineering decision thresholds for a specific sensor.

Future work should add Monte Carlo resistor tolerances, temperature-dependent resistance, source and amplifier models, analog-to-digital conversion, and experimentally measured noise. It should also compare absolute and ratiometric readouts, evaluate divider baseline subtraction, and report application-specific metrics such as signal-to-noise ratio, total error, power, cost, and bandwidth. These additions would allow a more complete practical comparison of the two circuit topologies.

Practical Guidance

Within the limitations above, a voltage divider remains reasonable when simplicity, low component count, or large resistance excursions dominate. A bridge is attractive when a near-zero differential baseline, differential amplification, and sensitivity to small fractional resistance changes are useful. Designers

should apply the framework with measured component data and the actual readout architecture rather than treating the ratio reported here as a universal rule.

For an application-specific decision, the model can be used as the first step in a larger error budget. A designer can replace the ideal resistances with measured values, restrict θ to the sensor's actual operating span, express ϕ using the source specification, and then add the gain and reference behavior of the converter. The resulting comparison may still favor a bridge, but the result would then be based on the requirements and nonidealities of the actual circuit.

CONCLUSION

This study derived and simulated a dimensionless metric that compares local sensitivity to normalized resistance change with local sensitivity to normalized excitation variation. For the specified ideal quarter-active bridge and voltage-divider outputs, the pointwise bridge-to-divider efficiency ratio is $2|1 + \theta|/|\theta|$, independent of φ. Over the sampled domain, the ratio ranges from 2.4 to 22 and averages 4.95. The advantage is largest near the balanced limit and narrows as resistance excursion increases.

The result should be interpreted as a property of the chosen model and metric. At exact balance, the ideal ratio is undefined rather than physically infinite, and real nonidealities remove the singular behavior. Ratiometric conversion, divider baseline subtraction, component tolerance, noise, and readout electronics can also change the practical comparison. The main contribution is therefore the analytical framework, which identifies the assumptions behind the observed advantage and provides a starting point for more realistic circuit-specific analyses.

DATA AND CODE AVAILABILITY STATEMENT

The complete Python code used to generate the numerical grids, summary statistics, and Figures 3–4 is reproduced in Appendix A. The study uses no external dataset.

ACKNOWLEDGEMENTS

The author thanks Benjamin Davis and RISE Research for guidance on project planning and scientific communication.

ABOUT THE AUTHOR

Tri Tran
Granada High School
Grade 12
Mentor: Benjamin Davis
Research program/affiliation: RISE Research

REFERENCES

M. Azadmehr, L. Marchetti, M. S. Elkharashi and Y. Berg, "A virtual Wheatstone bridge front-end for resistive sensors," 2017 IEEE 14th International Conference on Networking, Sensing and Control (ICNSC), Calabria, Italy, 2017, pp. 368-371, doi: 10.1109/ICNSC.2017.8000120.

B. Jan, M. Chavda, S. Sonuksale and S. Malik, "Thread based Resistive Sensor for Tactile and Slippage Detection in Smart Bionics," 2024 IEEE Applied Sensing Conference (APSCON), Goa, India, 2024, pp. 1-4, doi: 10.1109/APSCON60364.2024.10465895.

Chiang, C.-T., Chang, C.-M., & Chang, C.-C. (2018). Design of an ultraviolet light intensity monitor for personally wearable devices. *IEEE Sensors Journal*, 18(11), 4673–4678. https://doi.org/10.1109/JSEN.2018.2828023

De Marcellis, A., & Ferri, G. (2011). *Analog circuits and systems for voltage-mode and current-mode sensor interfacing applications*. Springer. https://doi.org/10.1007/978-90-481-9828-3

Harris, C. R., Millman, K. J., van der Walt, S. J., Gommers, R., Virtanen, P., Cournapeau, D., Wieser, E., Taylor, J., Berg, S., Smith, N. J., Kern, R., Picus, M., Hoyer, S., van Kerkwijk, M. H., Brett, M., Haldane, A., del Río, J. F., Wiebe, M., Peterson, P., … Oliphant, T. E. (2020). Array programming with NumPy. *Nature*, *585*(7825), 357–362. https://doi.org/10.1038/s41586-020-2649-2

Hunter, J. D. (2007). Matplotlib: A 2D graphics environment. *Computing in Science & Engineering*, *9*(3), 90–95. https://doi.org/10.1109/mcse.2007.55

Kester, W. (1999). Bridge circuits. In *Practical design techniques for sensor signal conditioning* (Section 2). Analog Devices. https://www.analog.com/media/en/training-seminars/design-handbooks/practical-design-techniques-sensor-signal/Section2.pdf

Liu, Y., Wang, H., Zhao, W., Zhang, M., Qin, H., & Xie, Y. (2018). Flexible, stretchable sensors for wearable health monitoring: Sensing mechanisms, materials, fabrication strategies and features. *Sensors*, *18*(2), 645. https://doi.org/10.3390/s18020645

Texas Instruments. (n.d.). *Bridge measurement systems* (Precision Analog Applications Seminar SLYP163). Texas Instruments. https://www.ti.com/lit/ml/slyp163/slyp163.pdf

Van Rethy, J., Danneels, H., De Smedt, V., Dehaene, W., & Gielen, G. E. (2013). Supply-noise-resilient design of a BBPLL-based force-balanced Wheatstone bridge interface in

130-nm CMOS. *IEEE Journal of Solid-State Circuits*, 48(11), 2618–2627. https://doi.org/10.1109/JSSC.2013.2274831

Wilson, D. M. (2022). Electronic interface circuits for resistance-based sensors. *IEEE Sensors Journal*, *22*(11), 10223–10234. https://doi.org/10.1109/jsen.2021.3124766

Yermoshin, N. I., Yakimov, E. V., Goldshtein, A. E., & Sednev, D. A. (2021). Increase in fast response time of the resistance-to-voltage converter when monitoring the cable products' insulation resistance. *Sensors*, *21*(2), 368. https://doi.org/10.3390/s21020368

Zhu, Y., Liu, Y., Sun, Y., Zhang, Y., & Ding, G. (2022). Recent advances in resistive sensor technology for tactile perception: A review. IEEE Sensors Journal, 22(16), 15635–15649. https://doi.org/10.1109/JSEN.2022.3179015

APPENDIX A. REPRODUCIBILITY CODE

The following listings reproduce the scripts used to generate the efficiency surfaces, summary values, and ratio map. Listings A1–A3 are unchanged. Listing A4 adds the reviewer-requested step-size check for Table 2.

Listing A1. figure3.py

```
import matplotlib.pyplot as plt
import numpy as np
# 1. Output Model Functions
def hdivider(theta, phi):
  return (1 + phi) * ((1 + theta) / (2 + theta))
def hbridge(theta, phi):
  return (1 + phi) * (((1 + theta) / (2 + theta)) - 0.5)
# 2. Derivative and Efficiency Functions
#  Voltage Divider
def numerator_voltagedivider(theta, phi):
  tinynumber = 0.0000000001
  numericalderivative = (
    hdivider(theta + tinynumber, phi) - hdivider(theta, phi)
  ) / tinynumber
  return np.abs(numericalderivative)
def denominator_voltagedivider(theta, phi):
  tinynumber = 0.0000000001
  numericalderivative = (
    hdivider(theta, phi + tinynumber) - hdivider(theta, phi)
  ) / tinynumber
  return np.abs(numericalderivative)
def Evoltagedivider(theta, phi):
  quotient = numerator_voltagedivider(theta, phi) / denominator_voltagedivider(
    theta, phi
  )
  return quotient
#  Wheatstone Bridge
def numerator_wheatstonebridge(theta, phi):
  tinynumber = 0.0000000001
  numericalderivative = (
    hbridge(theta + tinynumber, phi) - hbridge(theta, phi)
  ) / tinynumber
```

```
  return np.abs(numericalderivative)
def denominator_wheatstonebridge(theta, phi):
  tinynumber = 0.0000000001
  numericalderivative = (
    hbridge(theta, phi + tinynumber) - hbridge(theta, phi)
  ) / tinynumber
  return np.abs(numericalderivative)
def Ewheatstonebridge(theta, phi):
  quotient = numerator_wheatstonebridge(
    theta, phi
  ) / denominator_wheatstonebridge(theta, phi)
  return quotient
# 3. Parameter Grid
grid_divider = np.zeros((10, 15))
grid_bridge = np.zeros((10, 15))
thetavalues = np.linspace(0.1, 5, 10)
phivalues = np.linspace(0.1, 5, 15)
# Populate both efficiency grids in one nested loop
for k in range(0, 10):
  for j in range(0, 15):
    grid_divider[k, j] = Evoltagedivider(thetavalues[k], phivalues[j])
    grid_bridge[k, j] = Ewheatstonebridge(thetavalues[k], phivalues[j])
# 4. Side-by-Side 3D Plotting
A, B = np.meshgrid(thetavalues, phivalues)
Z_divider = grid_divider.T
Z_bridge = grid_bridge.T
# Create a wider figure to hold both 3D plots
fig = plt.figure(figsize=(14, 6))
#  Left Subplot: Voltage Divider
ax1 = fig.add_subplot(121, projection='3d')  # 1 row, 2 columns, 1st plot
surf1 = ax1.plot_surface(A, B, Z_divider, cmap='Blues')
ax1.set_title('Voltage Divider Efficiency')
ax1.set_xlabel('theta')
ax1.set_ylabel('phi')
ax1.set_zlabel('E')
fig.colorbar(surf1, ax=ax1)
#  Right Subplot: Wheatstone Bridge
ax2 = fig.add_subplot(122, projection='3d')  # 1 row, 2 columns, 2nd plot
surf2 = ax2.plot_surface(A, B, Z_bridge, cmap='Blues')
ax2.set_title('Wheatstone Bridge Efficiency')
ax2.set_xlabel('theta')
```

```
ax2.set_ylabel('phi')
ax2.set_zlabel('E')
fig.colorbar(surf2, ax=ax2)
plt.tight_layout()
plt.show()
```

Listing A2. figure4.py

```
import matplotlib.pyplot as plt
import numpy as np
#h(theta, phi)   [Eqs. (5)-(6)]
def hdivider(theta, phi):
  return (1 + phi) * ((1 + theta) / (2 + theta))
def hbridge(theta, phi):
  return (1 + phi) * (((1 + theta) / (2 + theta)) - 0.5)
#efficiency finite differences  [Eq. (4)]
#       E = |dh/dtheta| / |dh/dphi|
H = 1e-10  # finite-difference step
def efficiency(func, theta, phi):
  tinynumber = 1e-10
  d_theta = (func(theta + tinynumber, phi) - func(theta, phi)) / tinynumber
  d_phi = (func(theta, phi + tinynumber) - func(theta, phi)) / tinynumber
  return np.abs(d_theta) / np.abs(d_phi)
# 3. Parameter Grid & Data Generation
thetavalues = np.linspace(0.1, 5.0, 10)
phivalues = np.linspace(0.1, 5.0, 15)
ratio_grid = np.zeros((15, 10))
for i in range(15):
  for j in range(10):
     e_bridge = efficiency(hbridge, thetavalues[j], phivalues[i])
     e_divider = efficiency(hdivider, thetavalues[j], phivalues[i])
     ratio_grid[i, j] = e_bridge / e_divider
# 4. Plotting Setup
fig, (ax1, ax2) = plt.subplots(1, 2, figsize=(11.5, 4.6), dpi=300)
# --- Panel (a): Efficiency Ratio Map ---
pcm = ax1.pcolormesh(thetavalues, phivalues, ratio_grid, cmap='YlGn')
cb = fig.colorbar(pcm, ax=ax1, pad=0.02)
cb.set_label(r'R_E = E_bridge/E_div', fontsize=14)
cb.ax.tick_params(labelsize=12)
ax1.set_xlabel(r'θ  (normalized resistance variation)', fontsize=14)
ax1.set_ylabel(r'φ  (normalized voltage variation)', fontsize=14)
```

```
ax1.set_title('(a)  Efficiency-ratio map', fontsize=15, pad=8)
ax1.tick_params(labelsize=12)
# --- Panel (b): RE vs Theta ---
theta_fine = np.linspace(0.1, 5.0, 400)
closed_form_y = 2.0 * (1.0 + theta_fine) / theta_fine
ax2.plot(
  theta_fine,
  closed_form_y,
  '-',
  linewidth=2.4,
  label=r'Closed form  2|1 + θ|/|θ|  (Eq. 9)',
  zorder=1,
)
phi_targets = [0.1, 2.5, 5.0]
markers = ['o', 's', '^']
colors = ['#0e5c46', '#1a9e79', '#b8860b']
for phi_val, marker, color in zip(phi_targets, markers, colors):
  numerical_y = []
  for theta_val in thetavalues:
    ratio = efficiency(hbridge, theta_val, phi_val) / efficiency(
      hdivider, theta_val, phi_val
    )
    numerical_y.append(ratio)
  ax2.plot(
    thetavalues,
    numerical_y,
    marker,
    color=color,
    markersize=8,
    markerfacecolor='white',
    markeredgewidth=2,
    label=rf'Numerical, φ = phi_val',
    zorder=3,
  )
ax2.set_xlabel(r'θ  (normalized resistance variation)', fontsize=14)
ax2.set_ylabel(r'R_E', fontsize=14)
ax2.set_title(r'(b)  R_E is independent of φ', fontsize=15, pad=8)
ax2.set_yscale('log')
ax2.grid(True, which='both', linestyle=':', alpha=0.5)
ax2.legend(fontsize=11, framealpha=0.95)
```

```
ax2.tick_params(labelsize=12)
plt.tight_layout()
plt.show()
```

Listing A3. table_1_statistics.py

```
import numpy as np
def hdivider(theta, phi):
  return (1 + phi) * ((1 + theta) / (2 + theta))
def hbridge(theta, phi):
  return (1 + phi) * (((1 + theta) / (2 + theta)) - 0.5)
def efficiency(func, theta, phi, step=1e-10):
  d_theta = (func(theta + step, phi) - func(theta, phi)) / step
  d_phi = (func(theta, phi + step) - func(theta, phi)) / step
  return np.abs(d_theta) / np.abs(d_phi)
theta_values = np.linspace(0.1, 5.0, 10)
phi_values = np.linspace(0.1, 5.0, 15)
divider_grid = np.zeros((10, 15))
bridge_grid = np.zeros((10, 15))
for i, theta in enumerate(theta_values):
  for j, phi in enumerate(phi_values):
    divider_grid[i, j] = efficiency(hdivider, theta, phi)
    bridge_grid[i, j] = efficiency(hbridge, theta, phi)
ratio_grid = bridge_grid / divider_grid
def summary(values):
  return (
    np.max(values),
    np.min(values),
    np.mean(values),
    np.median(values),
    np.std(values),
  )
for label, values in (
  ("Voltage divider", divider_grid),
  ("Wheatstone bridge", bridge_grid),
  ("Pointwise ratio", ratio_grid),
):
  maximum, minimum, mean, median, population_std = summary(values)
  print(
    f"{label}: max={maximum:.12g}, min={minimum:.12g}, "
    f"mean={mean:.12g}, median={median:.12g}, "
    f"population_std={population_std:.12g}"
```

```
)
```

Listing A4. step_size_check.py

```
import numpy as np
def hdivider(theta, phi):
  return (1 + phi) * ((1 + theta) / (2 + theta))
def hbridge(theta, phi):
  return (1 + phi) * (((1 + theta) / (2 + theta)) - 0.5)
def efficiency(func, theta, phi, step):
  d_theta = (func(theta + step, phi) - func(theta, phi)) / step
  d_phi = (func(theta, phi + step) - func(theta, phi)) / step
  return np.abs(d_theta) / np.abs(d_phi)
theta = np.linspace(0.1, 5.0, 10)
phi = np.linspace(0.1, 5.0, 15)
T, P = np.meshgrid(theta, phi)
exact_div = (1 + P) / ((2 + T) * (1 + T))
exact_bridge = 2 * (1 + P) / (T * (2 + T))
exact_ratio = 2 * (1 + T) / T
print("NumPy:", np.__version__)
print("step, max relative error (%) for divider, bridge, ratio")
for step in (1e-4, 1e-6, 1e-8, 1e-10):
  div = efficiency(hdivider, T, P, step)
  bridge = efficiency(hbridge, T, P, step)
  pairs = ((div, exact_div), (bridge, exact_bridge),
       (bridge / div, exact_ratio))
  errors = [100 * np.max(np.abs(a / ref - 1)) for a, ref in pairs]
  print(step, *errors)
```